Int J Adv Manuf Technol (2013) 64:1445–1457
DOI 10.1007/s00170-012-4114-3

ORIGINAL ARTICLE

Influence of process parameters on impact toughness and hardness of dissimilar AISI 4140 and AISI 304 continuous drive friction welds

G. Subhash Chander · G. Madhusudhan Reddy · G. R. N. Tagore

Received: 12 August 2010 / Accepted: 27 March 2012 / Published online: 1 May 2012

Abstract Dissimilar joints between austenitic stainless steel and low alloy steel are extensively used in many high temperature applications in the energy conversion systems. In the present investigation, emphasis is made on the influence of process parameters on the impact toughness and hardness of the friction welded joints between these two materials. The important process parameters in friction welding such as friction force, forge force, and burn-off lengths are considered for optimization by Taguchi method using $L_8\ 2^7$ orthogonal array. It is found that under low friction force, forging force, and burn-off conditions, the impact toughness is high due to the observed acicular martensite. Low impact toughness is reported for the welds made at higher levels of the parameters. Carbon depletion is also observed close to interface in low alloy steel side. Microhardness at the weld center is less than the microhardness on either side at the interface of low alloy steel and austenitic stainless steel close to weld center. The contribution of each parameter and significance of interactions of these parameters is determined by Taguchi method. Among these parameters, friction force has significant influence and forging force has negligible influence on microhardness. The burn-off has maximum influence while forge force has minimum effect on toughness of the welds. Statistical analysis of variance is carried out, optimum process parameters are evaluated, and regression equations are obtained.

Keywords Friction welding · Dissimilar joints · Austenitic stainless steel · Low alloy steel · Impact toughness · Regression equation

G. S. Chander (✉)
Swarna Bharathi Institute of Science and Technology,
Khammam, AP, India
e-mail: gscmec@yahoo.com

G. M. Reddy
Defense Metallurgical Research Laboratory,
Khanchanbagh,
Hyderabad, AP, India

G. R. N. Tagore
National Institute of Technology,
Warangal, AP, India

1 Introduction

There is an extensive need for dissimilar metal joints in power plant components, due to the severe gradients in mechanical and thermal loading. In central power stations, the parts of the boilers that are subjected to lower temperature are made of low alloy steel for economic reasons. The other parts, operating at higher temperatures, are constructed with austenitic stainless steel. Therefore, transition welds are needed between these two materials. The joining of dissimilar material is generally more challenging than that of similar metals because of different physical, chemical, and metallurgical properties of the parent metals that are to be joined. In welding of dissimilar metals, the different problems to be considered are

1. Carbon migration from high carbon-containing alloy to low carbon-containing alloy
2. The differences in thermal expansion coefficient resulting in differences in thermal residual stresses across the different weldment region
3. Electrochemical property variations in weldments, resulting in environmentally assisted problems like corrosion
4. Dilution
5. Distortion

Table 1 Chemical composition of parent metal (%wt.)

Material	C	Si	Mn	P	S	Cr	Ni	Mo	Fe
AISI 304	0.06	0.32	1.38	0.04	0.28	18.4	8.17	0.5	Balance
AISI 4140	0.42	0.34	0.69	0.01	0.01	0.8	1.46	0.11	Balance

The specific problems associated with welding of austenitic stainless steel are formation of delta ferrite, sigma phase, stress corrosion cracking, and sensitization at the interface. These problems can be overcome by solid-state welding techniques. Among the solid-state welding processes, friction welding has been proven to be a reliable and economical method of joining similar or dissimilar metal combinations [1,2].

Determination of combination of optimum process parameters in general is the major area of interest for many researchers. Many people studied the effect of process parameters on the weld quality following traditional experimental techniques, i.e., by varying one parameter at a time while keeping other s constant [3]. This process is time consuming and calls for enormous resources. This situation can be improved by the use of Taguchi method which has become a powerful tool for improving productivity during research and development so that high quality product can be produced quickly at lower cost. This method also helps in identifying significant parameter among the many parameters by conducting relatively less number of experiments. Research works applying this method on casting and fusion welding processes have been reported in literature [4–6]. Optimization of process parameters using Taguchi method for low alloy steel (AISI 4140) and austenitic stainless steel (AISI 304) dissimilar joints by friction welding process hitherto is not reported and hence assumes significance.

Impact toughness of the joints is an important property in the industries like fossil-fired power plants, automotive engine valves, and machine parts. In the present, study impact toughness, microstructure, and microhardness of friction welded joints are investigated. The various process parameters involved viz. friction force, forge force, and burn-off lengths are considered for optimization. The statistical analysis of variance (ANOVA) is carried out; optimum process parameters, their contributions and interactions are evaluated and regression equation is obtained.

Table 2 Mechanical properties of parent metals

Material	UTS (MPa)	YS (MPa)	El (%)
AISI 304	600	250	58
AISI 4140	758	558	21.3

UTS ultimate tensile strength, *YS* yield strength, *El* (%) percent elongation

Table 3 Friction welding parameters and their levels

Parameter	Unit	Level 1	Level 2	Symbol
Friction force	kN	15	30	X_1
Forging force	kN	40	75	X_2
Burn-off	mm	4	10	X_3

2 Experimental details

2.1 Material selection

Considered for this study are 25-mm diameter rods of austenitic stainless steel and low alloy steel. The chemical composition of the material is given in Table 1, and their mechanical properties are given in Table 2, respectively.

2.2 Heat treatment

In order to get better toughness for the parent low alloy steel, AISI 4140, it is heated up to 850°C and maintained at that temperature for 30 min followed by oil quenching. Tempering is done by heating up to 540°C and maintaining at that temperature for 3 h followed by air cooling [7]

The specimens are made as per ASTM standards. Nital (5 % nitric acid in 1,000 ml methyl alcohol) is used as etchant for low alloy steel while aquarigia (hydrochloric acid and nitric acid at 3:1 ratio) is used as etchant for austenitic stainless steel side. A low magnification stereomicroscope of Leitz make was employed for observing the deformation in welds. To observe the crack path and microstructural features, Leitz optical microscope was employed. Fractographic examination was carried out under Leo scanning electron microscope. Hardnesss measurements are taken from stainless steel to low alloy steel side along with the axial direction across the weld using microhardness testing machine on Vickers scale using 300 g load. The electron probe microanalysis is used to determine elemental distribution across the joint.

A 150-kN continuous-drive friction welding machine is used to conduct the experiments. The number of trial runs is

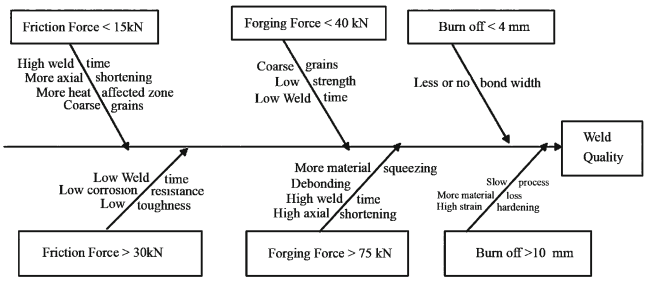

Fig. 1 Ishikawa diagram showing parameters and their effects

Table 4 Experimental layout of L_8 2^7 Orthogonal array

Expt. no	X_1	X_2	X_3	X_1X_2	X_1X_3	X_2X_3	$X_1X_2X_3$
1	−1	−1	−1	+1	+1	+1	−1
2	+1	−1	−1	−1	−1	+1	+1
3	−1	+1	−1	−1	+1	−1	+1
4	−1	−1	+1	+1	−1	−1	+1
5	+1	+1	−1	+1	−1	−1	−1
6	+1	−1	+1	−1	+1	−1	−1
7	−1	+1	+1	−1	−1	+1	−1
8	+1	+1	+1	+1	+1	+1	+1

made with various combination of friction force, forge force, and burn-off length, while others like brake delay time, feed rate, upset delay time, friction time, upset time, and rotational speed (1,500 rpm) are maintained constantly. Levels of these parameters are decided by inspecting the quality of weld in terms of cross-section, flash dimension, length loss, and defects if any.

The Ishikawa diagram as shown in Fig. 1 explains the limits of the process parameters as presented in Table 3. As shown in Fig. 1, three parameters of two levels each are used. The total degrees of freedom of each parameter and their interactions are 7; hence, the L_8 2^7 orthogonal array is selected and experiments are conducted as per the experimental layout given in Table 4.

3 Results and discussion

3.1 Visual inspection

Visual and stereo-microscopic examinations of the welds have revealed that the welds are of high quality and they are free from defects such as cracks, incomplete bonding, and other microstructural defects.

3.2 Torque, coefficient of friction, and power input characteristics

Figure 2 is the schematic sketch showing the variation in shortening, deformation, torque, speed, friction, and forging force with time during friction welding. From the friction welding machine, the report is obtained from the attached computer. From this report, it is obtained that peak torque and equilibrium torque decrease with decrease in friction force. The coefficient of friction is calculated using the formula T=.F.R/2, where "T" is the torque, "μ" is the coulomb coefficient of friction, "F" is the tangential frictional load (from Fig. 2), and "R" is the radius of the rod being welded [8]. Miltea and Radu [9] show that majority of the heat is generated at the annular space between1/3rd R to 2/3rd R.

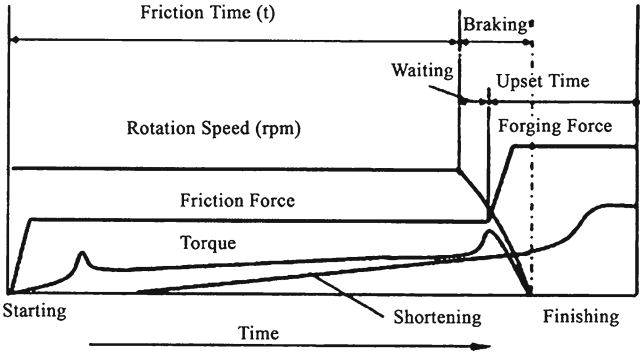

Fig. 2 Parameters on continuous drive friction welding

Hence, it is assumed that the resultant frictional load acts at the mid radius of the rod being welded. Table 5 gives the estimated coefficient of friction for peak torque, μ_p and coefficient of friction for equilibrium torque, μ_e in friction welding at different friction force conditions. Coefficient of friction is high during peak torque condition and reduces to a low value thereafter. This is attributed to heating and softening of the material during peak torque conditions. This argument is also in accordance with the findings of Celik et al. and Vikram Balasubramanian et al. [10,11].

The power input for the frictional heat generation is calculated by using $P=2\pi NT/60$, where "N" is the rotational speed in revolutions per minute. It is assumed that the heat generated during peak torque and equilibrium torque comprise 10 and 90 %, respectively. The power input rate is calculated by using P/t where "t" is the friction heating time presented in Table 5. The power input rate is high during high friction force condition and hence welding is fast. While the power input rate is low under low friction force condition and hence welding is slow. It is evident that the coefficient of friction at high friction force condition is less than the coefficient of friction at low friction force condition. It is attributed to high heat input rates at high friction force condition.

Table 5 Peak and equilibrium friction coefficients and power input rates

Expt. No	μp	μe	Power (P) (W)	10 % of power (P) (W)	Power (E) (W)	90 % of power (E) (W)	Total power (W)	Average welding time (s)	Power input rate (*W/s*)
1	0.64	0.32	9,292	929	4,646	4,181	5,111	40	127
2	0.34	0.19	9,912	991	5,575	5,018	6,009	22.2	283
3	0.49	0.31	7,124	712	4,491	4,042	4,754	43.2	110
4	0.43	0.26	6,195	619	3,717	3,345	3,964	124.6	91
5	0.34	0.18	9,912	991	5,265	4,739	5,730	22.6	254
6	0.32	0.18	9,292	929	5,111	4,500	5,429	33.42	162
7	0.48	0.25	6,969	697	3,526	3,206	3,903	79.6	49
8	0.32	0.17	9,292	929	4,956	4,460	5,389	34.8	155

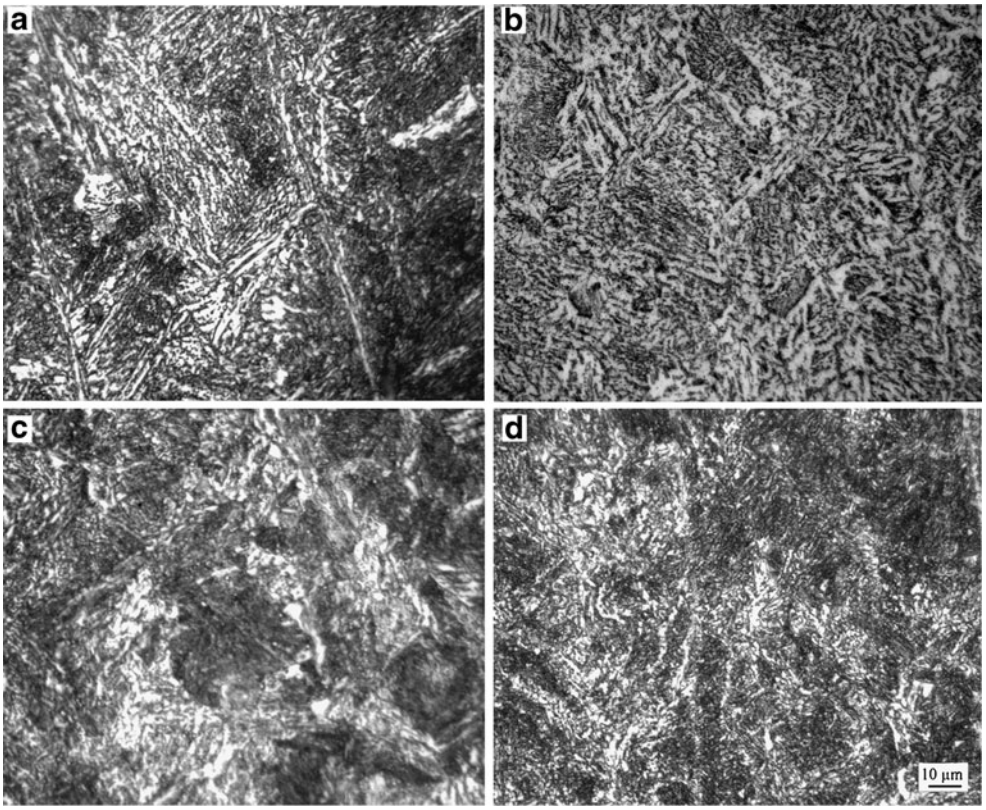

Fig. 3 Optical microstructures of low alloy steel side close to interface of the welds made under low friction force; **a** 15 (X_1)−40(X_2)−4(X_3), **b** 15(X_1)−75(X_2)−4(X_3), **c** 15(X_1)−40(X_2)−10(X_3), **d** 15(X_1)−75(X_2)−10(X_3)

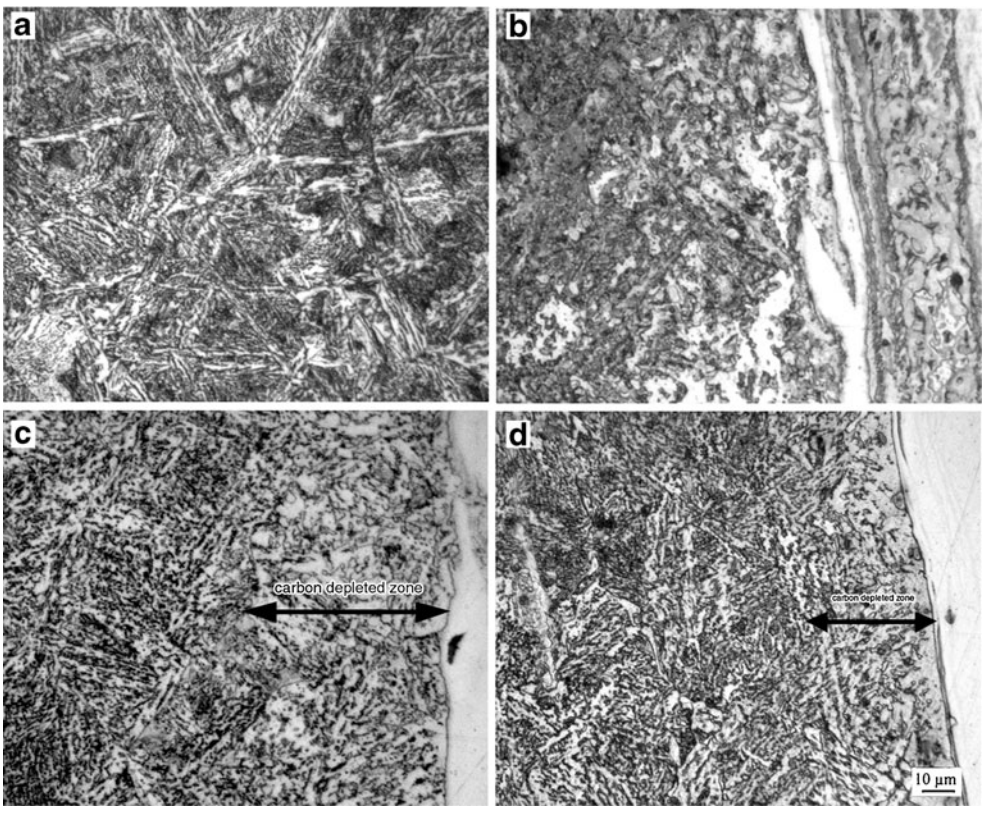

Fig. 4 Optical microstructures of low alloy steel side close to interface of the welds made under high friction force; **a** 30 (X_1)−40(X_2)−4(X_3), **b** 30(X_1)−75(X_2)−4(X_3), **c** 30(X_1)−40(X_2)−10(X_3), **d** 30(X_1)−75(X_2)−10(X_3)

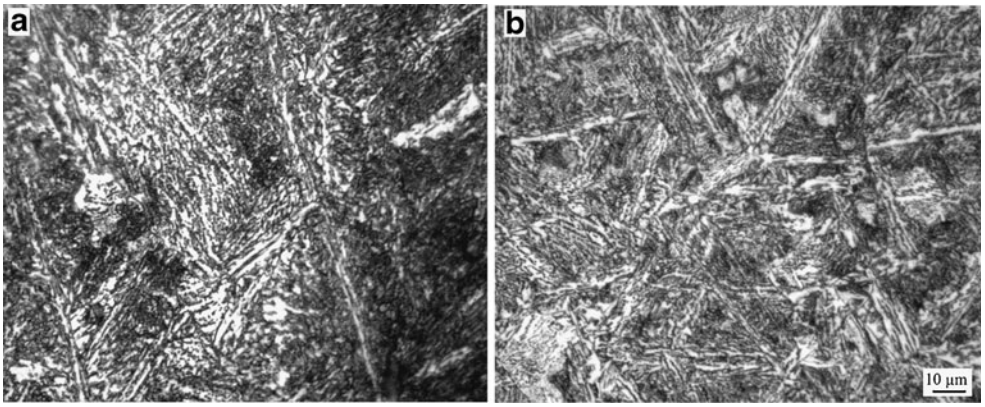

Fig. 5 Optical microstructures of low alloy steel side showing the effect of friction force; **a** weld at low friction force 15 (X_1)−40(X_2)−4(X_3), **b** weld at high friction force 30(X_1)−40 (X_2)−4(X_3)

3.3 Microstructural features of welded joints

The optical microsructures of weld at the interface of low alloy steel side under low friction force condition is given in Fig. 3. Owing to low heat input rate, high weld time, and slow cooling rate, the microstructure obtained is tempered martensite as shown in Fig. 3a. The optical microsructures of weld at the interface of low alloy steel side under high friction force condition is given in Fig. 4. Acicular martensite is produced due to high heat input rate and faster cooling rates as shown in Fig. 4a. Comparison of microstructure of weld at the interface of low alloy steel side under low friction and high force is given in Fig. 5 showing tempered martensite and acicular martensite.

However, under low friction force with high forging force, high burn-off, and both, the tetagonality of martensite is lost as shown in Fig. 3b–d, respectively, due to increased welding time. The microstuctures of welds at the interface of low alloy steel side with high friction force at high forging force, high burn-off, and both are shown in Fig. 4b–d, respectively. It is observed close to the interface, more clearly in high burn-off conditions; there is a depletion of carbon owing to high temperatures and high weld times. The effect of forging force on microstructure is shown in Fig. 6. Grain refinement is noticed as forging force is increased on the either side of the weld interface.

3.4 Microhardness

Microhardness of welds under the various combinations of process parameters along with the impact toughness and average weld time is given in Table 6. The typical

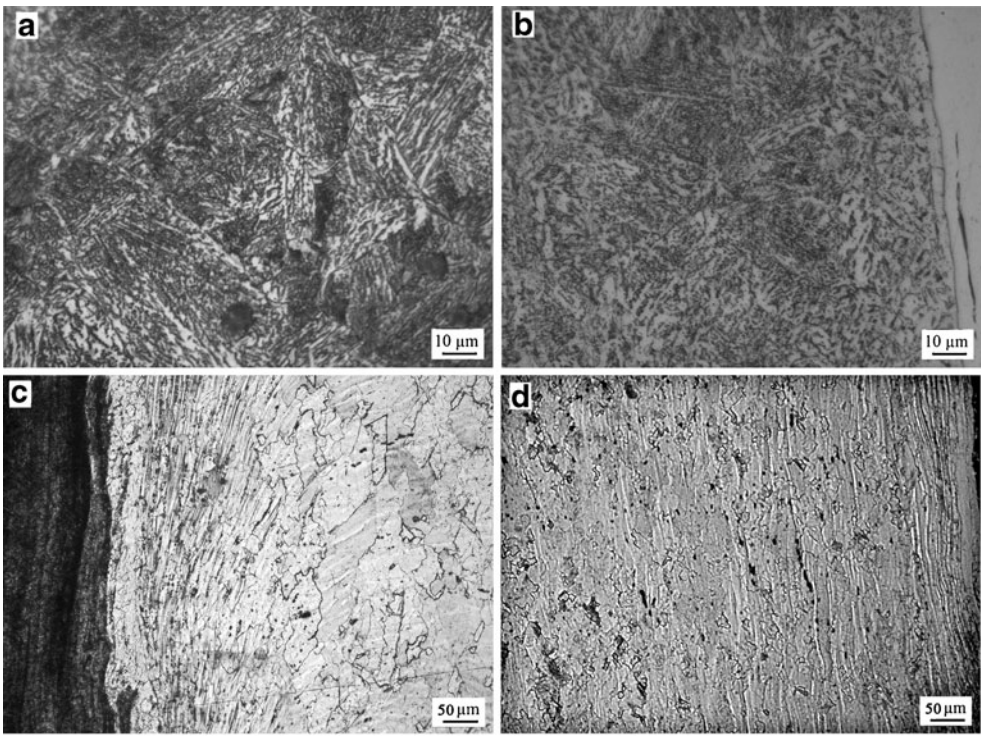

Fig. 6 Optical microstructure close to interface *i* on low alloy steel side; **a** 15(X_1)−40(X_2)−4 (X_3), **b** 15(X_1)−75(X_2)−4(X_3) *ii* on austenitic stainless steel side **c** 15(X_1)−40(X_2)−4(X_3) **d** 15 (X_1)−75(X_2)−4(X_3)

Table 6 Welding time and properties of friction welds

Expt. No	Welding time (s)				Impact toughness (J)				Microhardness (HV) at weld center			
	Trial 1	Trial 2	Trial 3	Average	Trial 1	Trial 2	Trial 3	Average	Trial 1	Trial 2	Trial 3	Average
1	39.4	40.5	40	40	41	43	43	42	357	360	348	355
2	22	22.2	22.4	22.2	36	35	36	35.7	405	410	397	404
3	42.8	43.2	43.6	43.2	38	36	37	37	358	355	362	358.3
4	124.6	123.5	125.7	124.6	24	27	26	25.7	325	320	331	325.3
5	21.8	22.6	23.4	22.6	32	28	30	30	412	415	399	408.7
6	33.1	33.7	33.42	33.42	12	14	12	12.7	371	375	367	371
7	79.1	80.1	79.6	79.6	25	21	24	23.3	316	310	321	315.7
8	34.8	35.3	34.28	34.8	13	11	13	12.3	370	377	365	370.7

microhardness profile of the friction weld made under 15–40–4 (friction force–forge force–burn-off) conditions are given in Fig. 7. In general, weld center is harder than parent metals. At the interface, two high hardness peaks with a drop in hardness in between is noted. The first peak is on the stainless steel side at the region consisting of deformed bonds close to interface. High strain hardening coefficient of stainless steel, presence of relatively more amount of Mo preventing softening at high temperatures and heavy deformation resulting work hardening are the reasons for high hardness of this region. The dip in hardness from peak value on stainless steel to low value at weld center is due to diffusion of Cr and Ni to the weld center as given in Fig. 8. This is also attributed to the softening of the material because of heat buildup as a result of low thermal conductivity of the material.

To the right of the interface, another peak is noted on the low alloy steel side because of the martensite. The dip in the

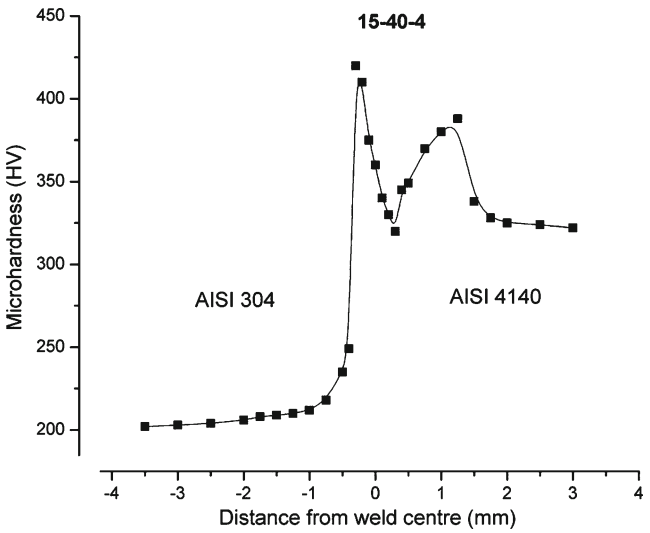

Fig. 7 Typical microhardness profile of weld under 15(X_1)−40(X_2)−4(X_3) condition

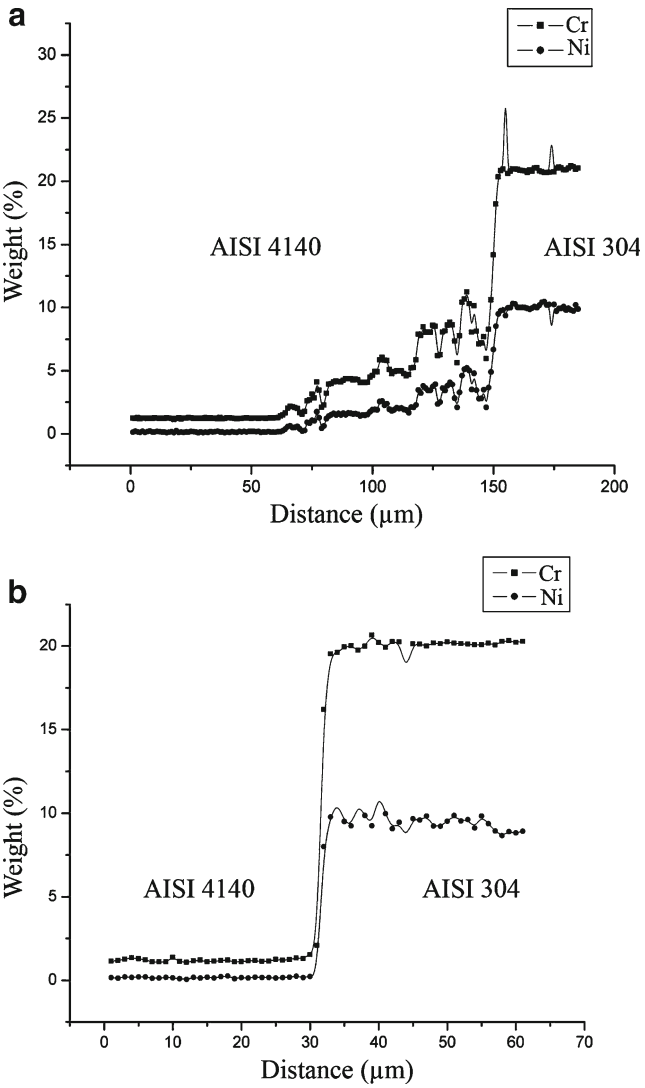

Fig. 8 Electron probe micro analysis across weld interface **a** 15(X_1)−40(X_2)−4(X_3), **b** 30(X_1)−75(X_2)−10(X_3)

Table 7 Microhardness at austenitic stainless steel interface, weld center and low alloy steel interface

Expt. no	Microhardness at ASS interface (HV)				Microhardness at weld center (HV)				Microhardness at LAS interface (HV)			
	Trial 1	Trial 2	Trial 3	Average	Trial 1	Trial 2	Trial 3	Average	Trial 1	Trial 2	Trial 3	Average
1	419	425	431	425	360	348	350	352	388	380	372	380
2	454	450	446	450	410	397	405	404	418	410	402	410
3	372	375	378	375	355	362	358	358	316	319	325	325
4	345	350	355	350	320	331	325	325	340	320	330	330
5	470	475	48	475	415	399	412	409	365	375	370	370
6	392	400	408	400	375	367	371	371	354	365	360	360
7	374	375	371	375	310	321	316	316	318	325	331	325
8	395	39	385	390	372	365	365	369	361	370	377	370

peak hardness from low alloy side at the interface to the weld center is attributed to the diffusion of carbon from low alloy steel side to weld center due to the presence of strong carbide-forming elements like Cr. Table 6 gives microhardness values at the weld center. The peak value of microhardness at the interface of austenitic stainless steel and low alloy steel close to weld center supporting this argument is given in Table 7. Locations of the microhardness close to interface on low alloy steel and austenitic stainless steel are shown in Fig. 9. Under high friction conditions due to rapid cooling, the hardness is high while under low frictional force conditions, hardness is low due to slow cooling. Microhardness indentations are shown in Fig. 10 along with microstructure of the interface of the low alloy steel close to weld center for welds made under 30–75–10 (friction force–forge force–burn-off) condition. Close to weld center, the indentation is coarse indicating less microhardness due to carbon depletion while at adjacent areas, the indentation is fine indicating high microhardness.

3.5 Impact toughness

Charpy 'V' notch impact toughness is recorded to be maximum at 43 J for welds joined under conditions of 15–40–4 (friction force–forge force–burn-off) while minimum recorded for welds joined under 30–75–10 (friction force–forge force–burn–off) conditions with 13 J. It is evident from the results that impact toughness of the joints is comparatively more under low friction force conditions than high friction force conditions. Under high friction force conditions, peak temperatures are attained in short time, compared to low friction force conditions. This argument is supported by higher heat input rates at higher friction force conditions as given in Table 5. Under high friction force conditions, higher heat input rates and low weld times result in rapid cooling of the material. This results in acicular martensite on low alloy steel side as given in Fig. 5b. This acicular martensite is hard, brittle, and parallel and interconnected hence low toughness. However, during low

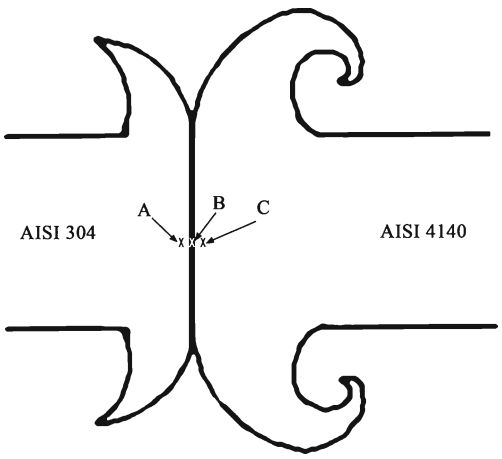

Fig. 9 Schematic sketch showing the microhardness at **a** close to interface on austenitic stainless steel side, **b** weld center, **c** close to interface on low alloy steel side

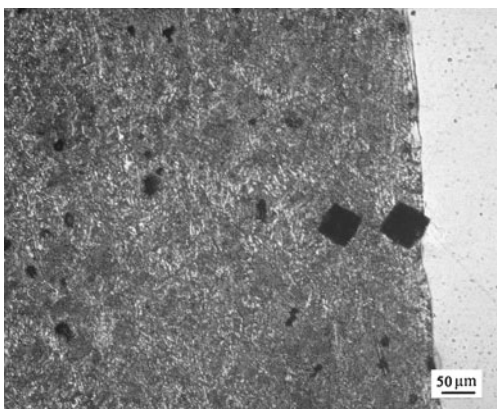

Fig. 10 Optical microstructure of low alloy steel side close to interface of the weld made under $30(X_1)-75(X_2)-10(X_3)$ conditions with microhardness indentations depicting low microhardness due to carbon depletion in weld

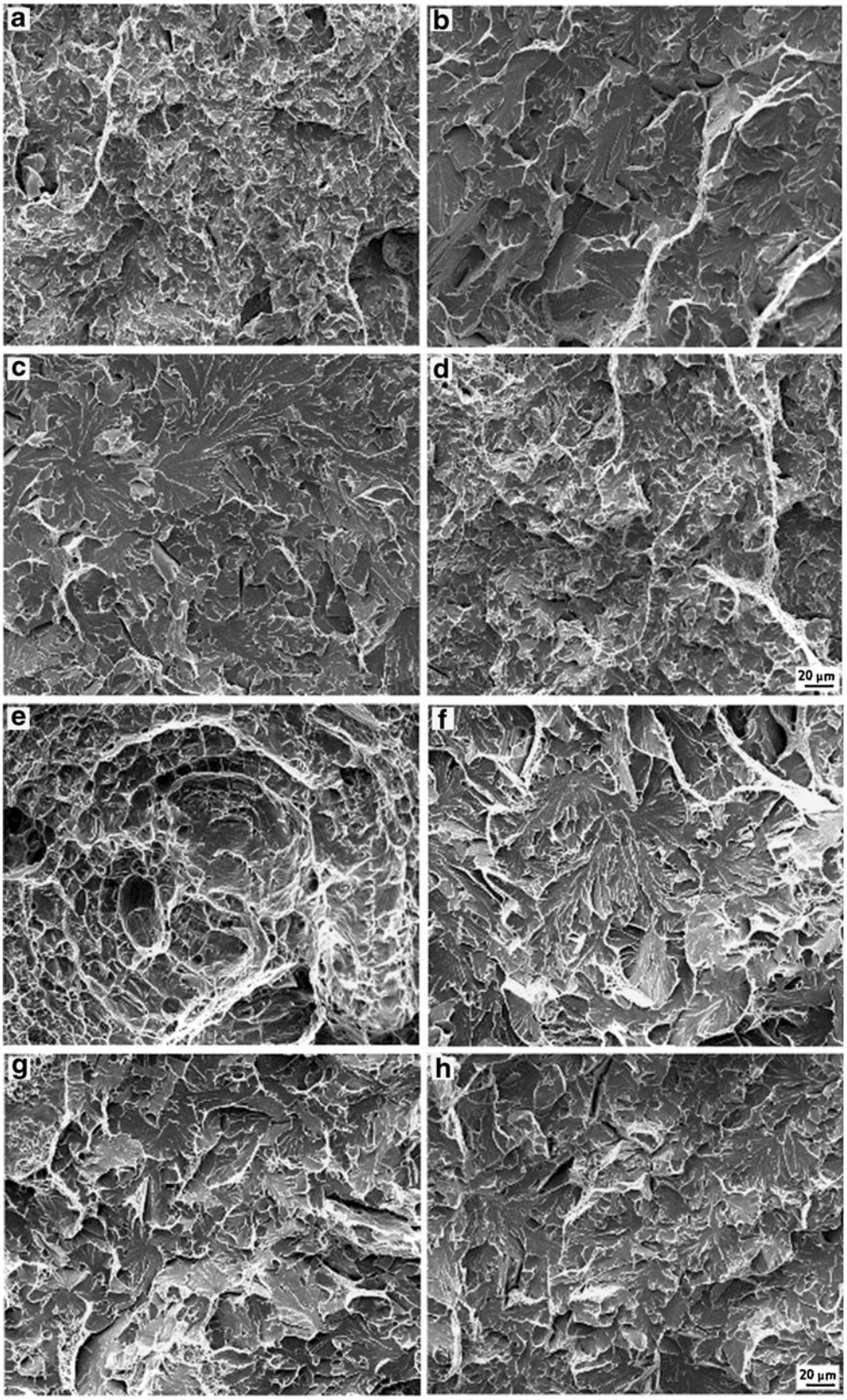

Fig. 11 Fracture features of impact samples at weld condition **a** 15–40–4, **b** 30–40–4, **c** 15–75–4, **d** 15–40–10

friction force conditions, heat input rates are low while weld times are high. High welding times result in tempering effect producing tempered martensite as depicted in Fig. 5a which is the reason for adequate toughness.

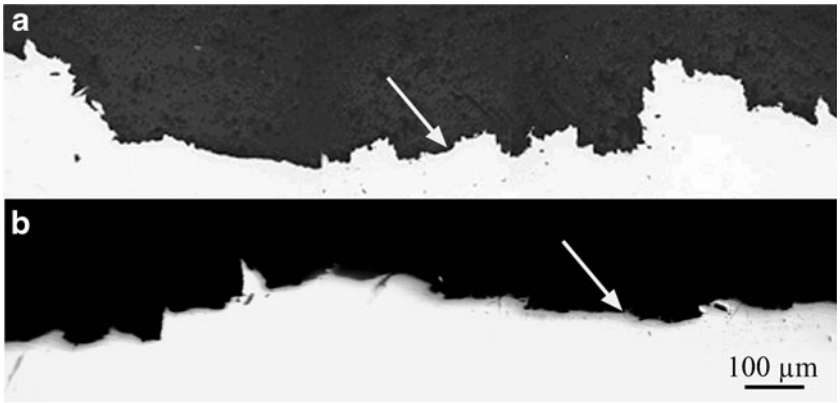

Fig. 12 Maximum crack path length was obtained for weld made under low frictional force condition while the crack path length is the minimum

Low impact toughness is noticed for welds made under high friction force with high forge force and high burn-off conditions. This may be attributed to carbon depletion as shown in Fig. 4b–d. Under low friction force conditions with high forge force and burn-off conditions, impact toughness decreased This may be attributed to low heat input and high weld times resulted in loss of tetragonality as shown in Fig. 3b–d.

The fractographic features as shown in Fig. 11 are in agreement with the above discussion. Though cleavage type of fracture is evident in all weld conditions under high friction force conditions, the cleavage facet size is more. Increase in the facet size indicates low energy fracture, which supports the decreasing trends in toughness.

The crack paths for low and high friction force conditions are obtained by cutting the impact samples perpendicular to the notch at the center. The maximum crack path length was obtained for weld made under low frictional force condition while the crack path length is the minimum as shown in Fig. 12 at high friction force condition. It was found that the crack is highly torturous in low friction force conditions than high friction force conditions. With improvement in toughness, the crack path length was more tortuous. These observations are in conformity with similar trends reported in steels and titanium alloys [12,13].

Under the same friction force and burn-off conditions, with increase in forging force, grain size refinement takes place [14] at the interface as shown in Fig. 6, despite of this the toughness is reduced by 5–10 %. As the weld zone grain size is finer, crack deviation at the grain boundaries would not be large as when it takes place in coarse grain structure. In addition, aligned microstructural features would offer less resistance to crack propagation. Similar trends are reported in ultrahigh strength steel, titanium alloys, and ferritic stainless steel at high forge force and burn-off conditions [15,16]. It has been reported that coarse grain sizes offer better toughness due to crack path deviation at large angles resulting in reduced stress intensity at crack tip [16–19].

3.6 Statistical analysis

The basis for this approach is the assumption of a simplified linear model for the optimization of output parameter μ given by

$$\mu = \alpha_0 + \alpha_1 x_1 + \alpha_2 x_2 + \ldots\ldots\ldots$$

Table 8 ANOVA table for Microhardness (Minimization)

Factor	Estimate (E)	Sum of squares (SS)	Degrees of freedom (DOF)	Mean squares (MS)	F	% Contribution	H_0
b_0	363.25						
b_1	24.88	9,900.3	1	9,900.3	148.3	64.0	Rejected
b_2	−0.25	1.0	1	1.0	0.01	0.01	Accepted
b_3	−17.5	4,900.0	1	4,900.0	73.4	31.68	Rejected
b12	1.13	20.3	1	20.3	0.3	0.13	Rejected
b23	−2.25	81.0	1	81.0	1.21	0.52	Accepted
b13	0.38	2.3	1	2.3	0.03	0.01	Accepted
b123	1.38	30.3	1	30.3	0.45	0.2	Accepted
SSR		14,935.0	7				
SSE		534.0	8				
SST		15,469.0	15				

Table 9 Regression equation, coefficient of correlation and optimum conditions for microhardness, Charpy V notch impact toughness, microhardness at austenitic stainless steel interface and microhardness at low alloy steel interface

Property	Regression equation	Coefficient of correlation (%)	Objective	Optimum conditions
Microhardness	$Y=363.13+25.00X_1-17.92X_3$	98.5	Minimization	$X_1(-1)\ X_2(0)X_3(+1)$
Impact toughness	$Y=27.38-4.71X_1-1.71X_2 -8.8X_3-1.04X_1X_3-1.29X_2X_3$	98	Maximization	$X_1(-1)X_2(-1)X_3(-1)$
Microhardness at austenitic stainless steel interface	$Y=401.5+27.5X_1-30X_3 +8.75X_1X_2-10.0X_1X_2X_3$	96.8	Minimization	$X_1(-1)\ X_2(0)X_3(+1)$
Microhardness at low alloy steel interface	$Y=361.63+26.63X_1-16.63X_3$	91.3	Minimization	$X_1(-1)\ X_2(0)X_3(+1)$

where, x_1, x_2 ….are the factors on which μ depend and α_0, α_1, α_2…. represents the true value of the corresponding unknown. From the results of an with finite number of trials, we can arrive at sample estimates of coefficients, a, which are then usually fitted into a linear regression equation of the type of

$$y = b_0 + b_1x_1 + b_2x_2 + \ldots.$$

where y is the response function and b_s are estimated values of α_s. In simple terms, each coefficient represents the influence of the corresponding factor on the output parameter.

Table 8 presents ANOVA for microhardness obtained using Mat Lab software. The contribution of each process parameter and their interaction influencing the quality of weld are evaluated based on ANOVA. Regression equation and coefficient of correlation for microhardness at the weld center, impact toughness, microhardness at austenitic stainless steel interface close to weld center, and microhardness at low alloy steel interface close to weld center are given in Table 9. Friction force has significant influence on microhardness with about 64 % contribution while burn-off has 31.7 % contribution. The influence of forge force is negligible. Microhardness decreases with decrease in friction force and increase in burn-off. Figure 13 gives the response graph of factors and their interaction for microhardness. The optimum conditions obtained are corresponding to low levels of friction force and high levels of burn-off. Similar trends are noted for microhardness at the interfaces of austenitic stainless steel and low alloy steel as given in Table 7. Signal-to-noise ratios for all parameters and their interactions are also calculated and presented in Table 10 for microhardness on smaller-the-better basis using the formula given below using Minitab software.

$$\text{S/Nratio}, \eta = -10\log_{10}[(1/n) \times \text{mean sum of squares of measured data}].$$

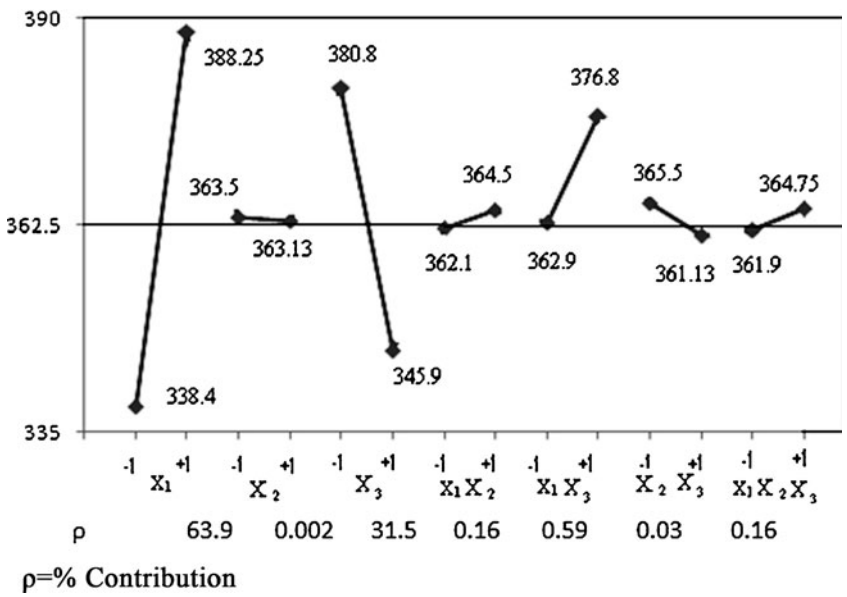

Fig. 13 Response graph of factors and their interactions of microhardness

Table 10 S/N response table for microhardness for minimization

Symbol	Parameter	S/N ratio		Difference	Rank[a]
		Level 1	Level 2		
X_1	Friction force	−50.6	−51.8	1.2	I
X_2	Forging force	−51.2	−51.2	0	VII
X_3	Burn-off	−51.7	−50.8	0.9	II
X_1X_2	Interaction effect	−51.22	−51.26	0.04	VI
X_2X_3	Interaction effect	−51.29	−51.12	0.17	III
X_1X_3	Interaction effect	−51.26	−51.21	0.05	V
$X_1X_2X_3$	Interaction effect	−51.2	−51.26	0.07	IV

[a] Rank indicates the significance of the parameter

Table 12 S/N response table for impact toughness for maximization

Symbol	Parameter	S/N ratio		Difference	Rank[a]
		Level 1	Level 2		
X_1	Friction force	36.37	33.99	2.38	II
X_2	Forging force	35.92	34.68	1.24	III
X_3	Burn-off	37.26	31.81	5.45	I
X_1X_2	Interaction effect	35.26	35.42	0.16	V
X_2X_3	Interaction effect	35.32	35.37	0.05	VI
X_1X_3	Interaction effect	34.93	35.7	0.77	IV
$X_1X_2X_3$	Interaction effect	35.26	35.42	0.16	V

[a] Rank indicates the significance of the parameter

Table 10 gives the rank of significant factors for microhardness on smaller-the-better basis using the above formula. The significance factors as given by their ranks are similar to that obtained by ANOVA. Table 11 presents statistical ANOVA for impact toughness obtained using Mat Lab software. The contribution of each process parameter and their interaction influencing the quality of weld are evaluated based on ANOVA. The optimum process parameter combinations, regression equation, and coefficient of correlation are evaluated and presented in Table 9. The regression equation indicates that the impact toughness is maximum for low levels of the parameters, 15–40–4 (friction force–forge force–burn-off). The burn-off has more significant effect on impact toughness contributing around 75.8 % and friction force has 19.2 % while contribution of forge force is insignificant. The coefficient of correlation is 0.98.

Signal-to-noise ratios for all parameters and their interactions are also calculated using Minitab software and presented in Table 12 for impact toughness on higher-the-better basis using the formula given below.

$$\mathrm{S/N ratio}, \eta = -10\log_{10}[\text{mean sum of squares of reciprocal of measured data}]$$

The most significant factors as given by their rank in Table 12 and obtained from ANOVA are the same. Response graph of factors and their interaction for impact toughness is shown in Fig. 14. According to these two methods, the optimum conditions obtained are the same and impact toughness of the joints is maximum corresponding to the lower limits of the parameters.

Table 11 ANOVA table for impact toughness (Maximization)

Factor	Estimate (E)	Sum of squares (SS)	Degrees of freedom (DOF)	Mean squares (MS)	F	% Contribution	H_0
b_0	27.6						
b_1	−4.6	333.1	1	333.1	409.9	19.2	Rejected
b_2	−1.2	22.6	1	22.6	27.8	1.3	Rejected
b_1	−9.1	1,314.1	1	1,314.1	1,617.3	75.8	Rejected
b_{12}	0.2	0.6	1	0.6	0.7	0.03	Accepted
b_{23}	−1.4	33.1	1	33.1	40.7	1.9	Rejected
b_{13}	1.2	22.6	1	22.6	22.8	1.3	Rejected
b_{123}	0.3	1.6	1	1.6	1.9		Accepted
SSR		1,727.4	7		0.09		
SSE		6.5	8				
SST		1,733.9	15				

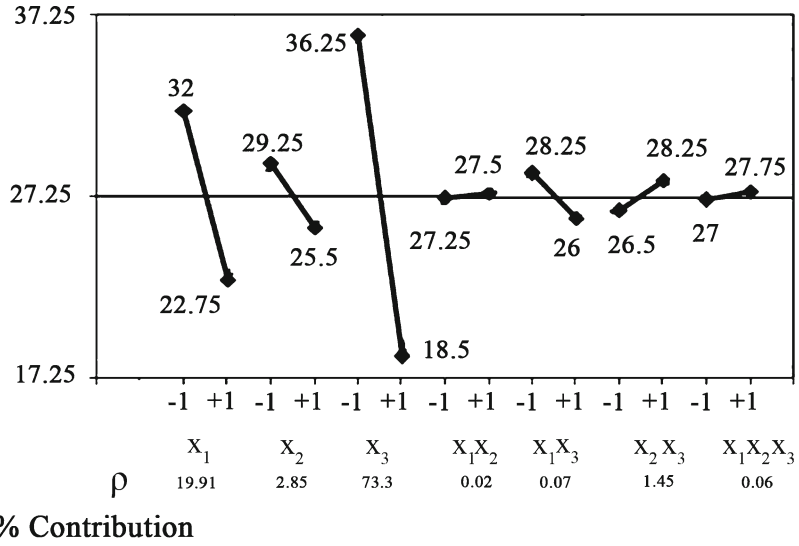

Fig. 14 Response graph of factors and their interactions of impact toughness

4 Conclusions

In this study, an attempt is made to determine the influence of the process parameters on impact toughness and microhardness of continuous drive friction welds of dissimilar metal AISI 4140 and AISI 304 steels. I t is found that

1. Peak torque and equilibrium torque decrease with decrease in friction force while power input rates increase with increase in friction force
2. Coefficient of friction is high during peak torque conditions and reduces to a low value thereafter. Coefficient of friction is high during low friction force condition and low for high friction force conditions
3. The impact toughness is the maximum under low frictional force, forge force, and burn-off conditions. Burn-off has a major role on the impact toughness, increase in burn-off decreases impact toughness, while forge force has insignificant role. The contribution of friction force on impact toughness is found to be about 20 %
4. Microhardness at the interface under low friction force condition is lower than higher friction force. This is because of tempering. The peak hardness in low alloy steel side and austenitic stainless steel side close to interface decreases with decrease in friction force

Acknowledgments We express our sincere gratitude to DRDO for the financial support to carry out this program. The authors are grateful to Dr. G. Malakondaiah, Director, DMRL for his constant encouragement. One of the authors (Mr. G. Subash Chander) is thankful to the Management, the Director and the Principal of SBIT, Khammam for support during this work.

References

1. Nicholas E D, Jessop TJ, Dindsdale WO (1978) Friction welding of dissimilar metals, advances in welding processes. Proceeding of 4th International Conference, New York 23
2. Jessop TJ, Dinsdale WO (1976) Mechanical testing of dissimilar metal friction welds. Weld Res Int 6:1
3. Lippold JC, Odegard BC (1984) Microstructural evolution during inertia friction welding of austenitic stainless steel. Weld J 63:355–389
4. Li WY, Ma TJ, Yang SQ, Xu QZ, Zhang Y, Li JL, Liao HL (2008) Effect of friction time on flash shape and shortening of linear friction welded 45 steel. Mater Lett 62:293–296
5. Juang SC, Tarng YS (2002) Process parameter selection for optimizing the weld pool geometry in tungsten inert gas welding of stainless steel. J Mater Process Technol 122:33–37
6. Anawa EM, Olabi AG (2008) Control of welding residual stress for dissimilar laser welded material. J Mater Process Technol 204:22–33
7. Balasubramanian M, Jayabalan V, Balasubramanian V (2008) Process parameter optimization of pulsed current argon tungsten arc welding of titanium alloy. Mater Technol 24:3
8. American Society for Metals (1987) Metals hand book, Ninth Edition, volume 4. p 121
9. Mitlea I, Radu B (1998) Thermal field numerical analysis in case of dissimilar materials, Mathematical modeling of weld phenomena 4. Materials modeling series. In:H Cerjak, HKDH Bhadeshia (eds). pp 444–453
10. Celik Sare and Ismail Ersozlu (2009) Investigation of mechanical properties and microstructure of friction welded joints between AISI 4140 and AISI 1050 steels. Mater Design 30:970–976
11. Balasubramanian V, Li Y, Stotler T, Crompton J, Soboyejo A, Katsube N, Soboyejo W (1999) A New Friction law for the modeling of continuous drive friction welding applications to 1045 steel. Mater Manuf Process 14(6):845–860
12. Rajashekar A, Madhusudhan Reddy G, Mohandas T, Murthy VSL (2008) Influence of post weld heat treatments on microstructure and mechanical properties of AISI 431 martensitic stainless steel friction welds. Int J Mat Sci Technol 24(2):202–212
13. Mohandas T, Banerjee D, Kutumbarao VV (1998) Observation on impact toughness of electron welds of $a+\beta$ titanium alloys. Mater Sci Eng A2:147–154

14. Yilmaz M, Karagoz S (1997) Joining of ceramics–metal parts by friction welding. National Welding Technology Congress, Ankara, Turkey. pp 207–19
15. Mohandas T, Kulkarni M S, Reddy G M (2003) Welding studies on super-duplex stainless steel. DMRL, Defense Metallurgical Research Laboratory, Hyderabad, India TR 338: 1–34
16. Kawabe Y, Muneki S, Takahashi J (1983) Grain size dependence of fracture toughness in ultra high strength maraging steel. J Iron Steel Inst 69:145–151
17. Breslaner E, Rosen A (1991) Relationship between microstructure and mechanical properties of metastable ß titanium 15–3 allloy. Mater Sci Technol 7:441–444
18. Satyanarayana VV, Reddy GM, Mohandas T, Rao GV (2003) Continuous drive friction welding studies on AISI 430 ferritic stainless steels. Sci Technol Welding Joining 8(8):184–193
19. Nimoni M, Kobayashi T, Sasaki N (1988) Toughness and microstuctural factors of Ti-6Al-4V alloy. Mater Sci Eng 100:45–55